Predicting Flood Inundation Depth Based-on Machine Learning and Numerical Simulation

Adriano, Bruno
Yokoya, Naoto
Yamanoi, Kazuki
Oishi, Satoru

Predicting Flood Inundation Depth Based-on Machine Learning and Numerical Simulation

Bruno Adriano[1,*], Naoto Yokoya[2,1], Kazuki Yamanoi[3] and Satoru Oishi[4]

[1]RIKEN Center for Advanced Intelligence Project, Tokyo 103-0027, Japan
[2]Department of Complexity Science and Engineering, The University of Tokyo, Chiba 277-8561, Japan
[3]Disaster Prevention Research Institute, Kyoto University, Kyoto 612-8235, Japan
[4]RIKEN Center for Computational Science, Kobe 650-0047, Japan

Abstract

Recent advances in earth observation and machine learning have enabled rapid estimation of flooded areas following catastrophic events such as torrential rains and riverbank overflows. However, estimating the actual inundation depth remains a challenge since it often requires detailed numerical simulation. This paper presents a methodology for predicting the inundation from remote sensing derived information by coupling deep learning and numerical simulation. We generate a large dataset of flood depth inundations considering several heavy rain conditions in four independent target areas. We propose a CNN-based regression framework. Our experiment demonstrates that our methodology can predict inundation depth on a separate target area not included during training, demonstrating great generalization ability.

Keywords

Flood inundation, machine learning, earth observation, numerical simulation

1. Introduction

Flood disasters can generate significant socioeconomic impacts [1]. Recent studies on flood events indicate climate change has increased river overflow primarily due to the increase of rainfall in certain regions [2]. Accurate flood extent maps are an immediate requirement for damage assessment. Currently, most remote sensing-based techniques for rapid mapping limit their analysis to grasp the spatial extent of flood [3]. However, from the decision-making point of view, having the flooded extent might not be enough information to develop an efficient response plan, especially in cases where the flooded areas are extensive and relief resources are limited.

In this paper, we propose a methodology for estimating inundation depth in the case of flood disasters, using an integration of numerical simulation and convolutional neural networks (CNNs) technologies. Our method is an extension of the framework presented in [4]. Similarly, we conduct numerical simulations of several artificial heavy rainfall scenarios to generate training data that include maximum inundation depth and derived flood extent, represented as binary mask images. A CNN-based regression model links remote sensing-derived information such as digital elevation model (DEM) and flood extents to the corresponding inundation depth distribution. In a development scenario, CNN models are trained in advance. Then, in the deployment phase, after a disaster has occurred, we can rapidly forecast the inundation depth using mainly two parameters DEM and flooded areas.

Our proposed methodology represents an advance for rapid flood disaster response methods. Current techniques limit their scope to estimate the flood extent. Our approach adds extra information to the disaster response in the form of inundation depth. The main contributions of this work are threefold, which are as follows.

1. We propose a methodology that integrates deep learning (CNN models) and numerical simulation to estimate inundation depth distribution after flood disasters. The framework uses simulation results to generate training data for the CNN models.
2. We construct four datasets for our methodology based on previous events that occurred at different locations in Japan. Each site presents unique features in terms of its land surface, resulting in complex patterns of flood disasters.
3. We conduct extensive experiments and evaluate the performance of our flood mapping approach in a test area independent of the training datasets.

CDCEO 2022: 2nd Workshop on Complex Data Challenges in Earth Observation, July 25, 2022, Vienna, Austria
*Corresponding author.
bruno.adriano@riken.jp (B. Adriano);
yokoya@edu.k.u-tokyo.ac.jp (N. Yokoya);
yamanoi.kazuki.6s@kyoto-u.ac.jp (K. Yamanoi);
tetsu@phoenix.kobe-u.ac.jp (S. Oishi)
0000-0002-4318-4319 (B. Adriano); 0000-0002-7321-4590 (N. Yokoya); 0000-0002-9421-8566 (K. Yamanoi); 0000-0002-9421-8566 (S. Oishi)

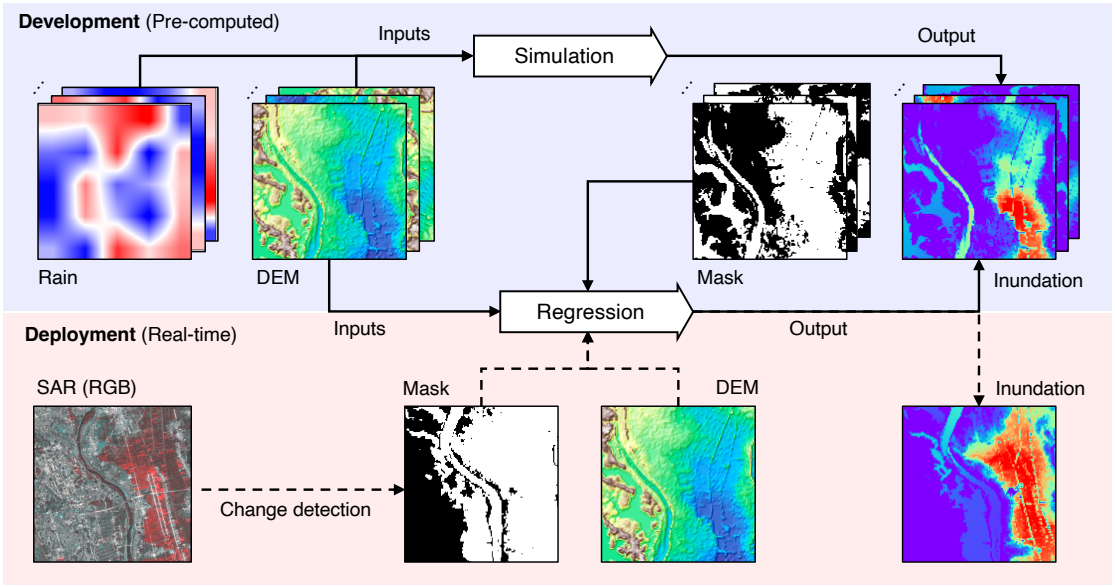

Figure 1: Overview concept of the proposed framework.

2. Related Work

2.1. Flood mapping via remote sensing

Flood detection is a well-studied topic in the remote sensing community. Pioneer methods are based on moderate and high-resolution optical imagery, exploiting their multi-spectral information. These methods primarily utilize the near-infrared band to compute spectral indexes such as the well-known Normalized Difference Vegetation Index (NDVI). For instance, [5] analyzed images from the Terra-ASTER and Ikonos sensors to estimate the flood extent after the 2004 Indian Ocean Tsunami. They accurately detected the flood areas in southern Thailand. However, one drawback of using optical sensors is that they are susceptible to weather and day-light conditions. Thus cloudy skies render optical images almost unusable.

With advances in earth observation technologies, such as Synthetic Aperture Radar (SAR), several researchers have developed efficient algorithms to detect flooded areas using change detection analysis of images acquired before and after the disaster. For instance, [6] evaluated the ability of fully-parametric SAR data to detect flooded areas after the 2011 Tohoku Tsunami. [7] presented an index-based analysis using multi-temporal statistics of SAR images.

Following the success of modern machine learning algorithms, several end-to-end methods have been proposed using either optical imagery of SAR data. For instance, [8, 9, 10] developed techniques for assessing flood extent using SAR intensity and coherence data and advanced CNN-based frameworks. Recently, [4] presented a novel framework that integrates remote sensing analysis and deep learning models. Their methods successfully estimate flood and the associated debris-flow in case of disaster due to torrential rainfalls.

2.2. Flood Analysis via Numerical Simulation

In general, methods based on numerical simulation give better accuracy for estimating flood extent and its corresponding inundation depth. These methods often involve expensive computation to solve complex physical-based governing equations [11]. As such, numerical simulation methods are primarily used to develop risk maps considering extreme scenarios [12] as preparation for future disaster events.

3. Methodology

This study integrates two advanced technologies, namely numerical simulation and deep learning. The numerical simulation generates sufficient training samples, and deep learning maps the nonlinear relationship present in the training data. Our proposed methodology presents two main modules. First, in the development stage, we synthesize a sufficient amount of training samples of flood inundation using a physical-based numerical model. Then, we train a CNN model in a regression setting to map a binary mask representing the flooded area and

DEM to the corresponding inundation depth. Second, deployment stage, we assume that following a significant flood disaster, it is possible to obtain the flooded area (binary mask) through the analysis of remote sensing imagery (e.g., Synthetic Aperture Radar, optical imaging). Then, using the binary mask and DEM as inputs, we can infer the associated inundation depth based on the CNN model trained in the first stage. Fig. 1 depicts an overview of our proposed framework. In this paper, we primarily focus on testing the concept of the first stage and present a preliminary evaluation of the second stage.

3.1. Flood simulation

In this work, we use the Rainfall-Runoff-Inundation (RRI) Model developed by the International Center for Water Hazard and Risk Management (ICHARM). The RRI model is capable of simulating rainfall-runoff and flood inundation simultaneously in a two-dimensional configuration [13]. The RRI model handles the terrain slope and river channels separately. In its 2D configuration, the channels are discretized as the center line of the overlying slop grid cell. The flow on the grid terrain slope is calculated using the 2D diffusive wave model, while the river channel flow uses a 1D diffusion wave model.

$$\frac{\partial h}{\partial t} + \frac{\partial q_x}{\partial x} + \frac{\partial q_y}{\partial y} = r - f \tag{1}$$

$$\frac{\partial q_x}{\partial t} + \frac{\partial \mu q_x}{\partial x} + \frac{\partial \nu q_x}{\partial y} = -gh\frac{\partial H}{\partial x} - \frac{\tau_x}{\rho_w} \tag{2}$$

$$\frac{\partial q_y}{\partial t} + \frac{\partial \mu q_y}{\partial x} + \frac{\partial \nu q_y}{\partial y} = -gh\frac{\partial H}{\partial y} - \frac{\tau_y}{\rho_w} \tag{3}$$

The model's governing equations (Eqs. 1, 2, and 3) are derived from a mass balance and momentum conservation conditions. Where h is the height of water from the local surface, q_x and q_y are the unit width discharges in x and y directions, μ and ν are the flow velocities in x and y directions, r is the rainfall intensity, f is the infiltration rate, H is the height of water from the datum, ρ_w is the density of water, g is the gravitational acceleration, and τ_x and τ_y are the shear stresses in x and y directions, respectively.

The RRI model generally uses rainfall and DEM to forecast the corresponding inundation depth. Our methodology generates the synthetic flood inundation depth images using several precipitation scenarios generated randomly. For each target site, we defined thirty rainfall scenarios ranging from 0 mm/hr to 20 mm/hr. The maximum rain amount was set based on the historical record from all target sites.

In addition, we use a standard method [14] to derive the inundation depth based on the DEM and binary mask.

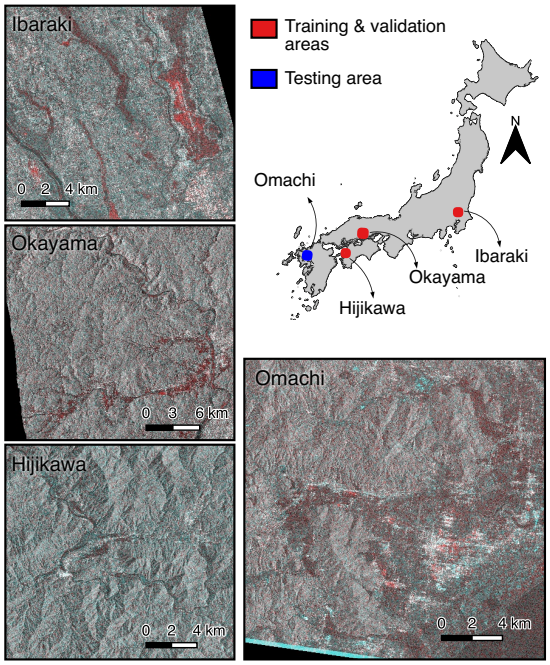

Figure 2: Flood disasters use in this study. The red square depicts the events used for training and validation of the CNN models. The blue square shows the event's location used for testing our proposed methodology.

This straightforward method finds the maximum floodwater level in the flooded area and subtracts it from the local inundated land elevation. This inundation depth (FwD) represents a theoretical assumption of a steady horizontal floodplain. We use this theoretical floodplain as a baseline to compare the performance of our methodology.

3.2. Deep-learning-based regression

Recently, CNN models have achieved excellent success in mapping nonlinear features as regression tasks [4, 15]. Here, we define the regression problem from DEM and flooded area to corresponding simulated inundation depth.

As described in the previous section, the inundation depth images are built using a numerical simulator using DEM and rainfall information as input. Further, we can generate the flooded area (binary mask) using the computed inundation depth by a straightforward thresholding approach. Here, we define flooded areas with an inundation depth greater than 0.2 m. Then, our regression models learn the nonlinear mapping f_θ from input x, which is consist of binary mask and DEM images, to output y (inundation depth): $f_\theta : x \rightarrow y$

As suggested by [4], we also use the smooth L_1 loss

(Huber loss) (Eq. 4, where $a = y - f_\theta(x)$ and $\delta = 1$) to optimize our CNN regression models. The Huber loss combines the advantage of the L2 loss (gradient decreases when the loss gets close to local minima) and the L1 loss (less sensitive to outliers).

$$\mathcal{L}_\delta(a) = \begin{cases} \frac{1}{2}(a)^2, & |a| \leq \delta \\ \delta|a| - \frac{1}{2}\delta^2, & \text{otherwise.} \end{cases} \quad (4)$$

For the regression tasks, we investigate a well-established encoder-decoder architecture (U-Net [16]), which has consistently shown high performance in semantic segmentation tasks [17], and two of its variations. First, the Attention U-Net [18] incorporates a self-attention mechanism in U-Net with contextual information extracted at a coarser scale. The attention module emphasizes accurate features for a given task and suppresses irrelevant features when concatenating features extracted by the encoder with those of the decoder through the skip connections. Second, the LinkNet [19] also has an encoder–decoder structure with residual blocks and skip connections, but it shares the information learned by the encoder with the decoder through additive operations. In the U-Net model and its variations, the overall design of each encoder block is two convolutional layers, each followed by batch normalization and a rectified linear unit (ReLU).

Finally, we use the Adam solver [20] for optimization with a learning rate of 0.0001. Xavier initialization is used to initialize the weights. The batch size is 64, and the number of epochs is 120. We use the PyTorch framework [21] to implement our CNN models in two NVIDIA TITAN RTX 24-GB GPUs.

4. Experiments

Here, we show the efficiency of our proposed methodology for predicting inundation depth using information collected from previous flood disasters in Japan. We evaluate the performance of the CNN-based models (e.i., U-Net, Attention U-Net, and LinkNet) using a realistic operational scheme.

4.1. Dataset

Our experiments focus on the flood disasters from four different events located at unique sites in Japan: 1) 2015 Floods in Ibaraki, 2-3) 2018 Floods in Okayama and Hijikawa, and 4) 2019 Floods in Omachi. All flood disasters occurred following torrential rainfalls. Fig. 2 shows the location of each event. The morphology of each target site is different, where Ibariki and Omachi present a gradually plain surface while Okayama and Hijikawa show mountain terrain.

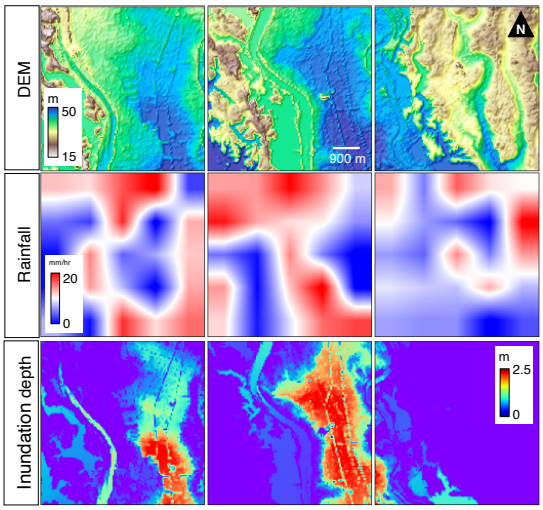

Figure 3: Examples of the inputs (DEM and rainfall) and outputs (maximum inundation depth) of the RRI model.

For the inundation depth simulation, we used the DEM released by the Geospatial Information Authority of Japan (GSI). GSI provides DEM of 5 m and 10 m grid size. In this study, to reduce the computational time, we construct the input DEM raster using a re-sampled ground sampling distance of 45 m. In addition to the DEM input, the RRI model requires the flow accumulation and flow direction that are directly calculated from the DEM. We use the ArcGIS 10.5 software to derive the later flow parameters.

We generate thirty rainfall scenarios for each target site to build the training samples. Then, the RRI model simulated each scenario and estimated the maximum inundation depth in meters. Here, we systematically crop, using a sliding window, tile where there is at least 0.2 m of inundation depth for each target area. This process eliminates spots with no inundation, such as mountain areas. We set the tile size as 5.76 km $\times$ 5.76 km (128 $\times$ 128 pixels). Finally, the tiles (samples) are 153, 253, 298, and 327 for Ibaraki, Okayama, Hijikawa, and Omachi, respectively. Fig. 3 shows examples of the simulated inundation depth using the RRI model.

4.2. Cross-domain evaluation

We use the root-mean-square error (RMSE) to evaluate our results. We compute a pixel-wise RMSE using the predicted inundation depths from the trained CNN models and the reference simulation results. Conventionally, machine learning methods evaluate their performance using training and testing samples derived with the same statistical distribution. Although such a scheme benefits model generalization, it does not represent a practical

Table 1
Numerical evaluation results in the validation dataset during model training.

Model	DEM + Mask	DEM + Mask + FwD
UNet	0.2201 $\pm$ 0.1712	0.2231 $\pm$ 0.1509
Att. UNet	0.2042 $\pm$ 0.1553	0.2053 $\pm$ 0.1514
LinkNet	0.2019 $\pm$ 0.1623	0.2164 $\pm$ 0.1608

application, especially in analyzing flood disasters where rainfall distribution and topographic features generate a unique pattern of inundation depth.

Thus, we design our experiments considering a real-world deployment. We used three target areas for training and validating our CNN models. Then, we tested the model performance and generalization using an independent test target area. These experiment settings represent a realistic condition during disaster response, where we can derive binary masks (flooded areas) using image analysis of remote sensing imagery or machine learning-based methods [22, 23]. Then, the DEM and binary mask are input for forecasting the expected inundation depth within the flooded area.

In this study, we select the Omachi area for testing our methodology. This area is never used in model training. Thus, we train the CNN models using the other target areas (i.e., Ibaraki, Hijikwa, and Okayama). We randomly split the remaining samples into two subsets, training and validation sets. We analyze the robustness of our framework by conducting three independent experiments using a different seed number to control the random operations. We report the mean and standard deviation of the three-fold experiments.

We conduct two training schemes. In the first, we construct the input images by concatenating the DEM and binary mask. This scheme represents a more realistic scenario. In the second training scheme, we also concatenate the theoretical floodplain (FwD). Thus the input image is a 3-channels raster. The purpose of the later scheme is to evaluate the accuracy of the CNN model by providing it with more information related to the inundation depth.

4.2.1. Quantitative Results

Table 1 shows the numerical results of predicting the inundation depth on the validation subsets. All three regression models perform similarly, with LinkNet slightly outperforming the other models. These results indicate that the networks successfully learn a nonlinear mapping from different binary change and DEM images to their corresponding inundation maps. These results are consistent with the training strategy of randomly split training and validation samples from the same statistical distribution, namely training target areas.

Furthermore, we also observe that including the FwD (theoretical floodplain) in the input does not significantly modify our models' performance. One possible reason for such an outcome is that the FwD is almost a linear operation of the DEM and binary mask. Thus, the information that it might input to the network is already included in the two other features (i.e., DEM and binary mask).

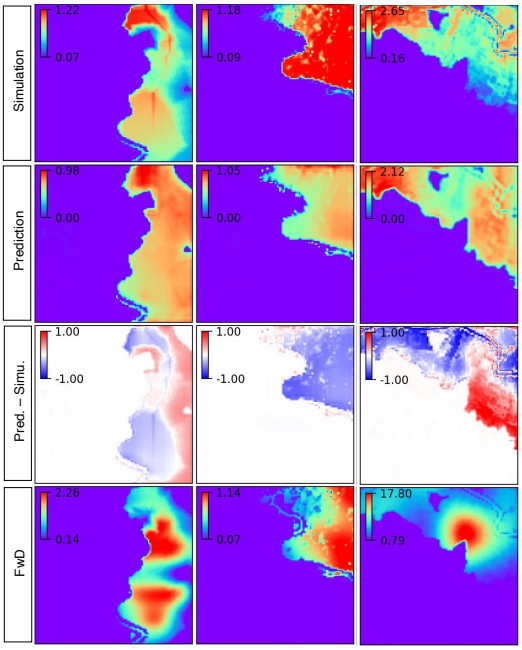

Figure 4: Prediction results from the test area (Omachi). From top to bottom are the reference inundation depth (simulated), the inferred inundation from the trained CNN models, the difference between prediction and reference inundation depth, and the theoretical floodplain.

Table 2
Numerical results of applying the trained model to the test site (Omachi area).

Model	DEM + Mask	DEM + Mask + FwD
UNet	0.1761 $\pm$ 0.1912	0.1781 $\pm$ 0.1209
Att. UNet	0.1532 $\pm$ 0.1553	0.1543 $\pm$ 0.1114
LinkNet	0.1419 $\pm$ 0.1023	0.1424 $\pm$ 0.0908

Table 2 list the numerical evaluation on the test target area (i.e., Omachi area). Recall that this area was never used during training, representing a fully out of the distribution set. We found that the LinkNet again shows slightly better performance among the different CNN-based regression models. However, in general, the models outperform the validation scores, demonstrating our framework's great generalization ability. One possible reason for such results is that the topographic

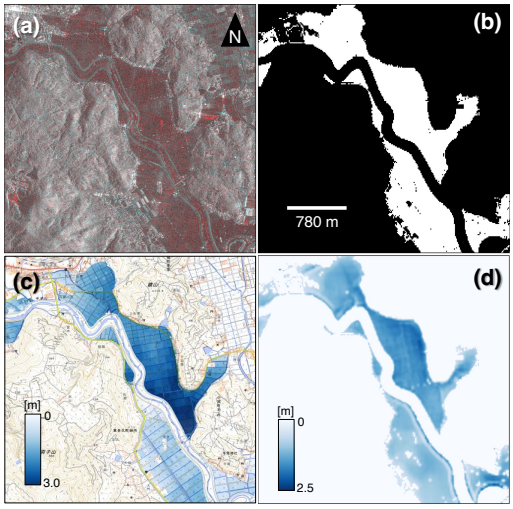

Figure 5: Application of our method to an actual event (2019 Heavy Rain in Kyushu, Japan). (a) RGB color composite of pre- and post-event ALOS-2 SAR data (R: pre-disaster and G B: post-disaster). (b) Flooded area binary map that can be estimated from (a). (c) Visual interpretation of the actual inundation published by GSI. (d) Predicted inundation depth using the binary map in (b) and DEM data.

characteristics of the Omachi test area might be included in the three training sites. Thus, the networks generalize when inferring the unseen site. This funding indicates that it is possible to develop a nationwide flood inundation mapping model by including a few key target areas with different topographic conditions.

Fig. 4 depicts the prediction results from the test area (Omachi). Here, the inundation patterns are consistent with the reference inundation (simulation results). Further, the difference between the prediction results and reference inundation indicates that the network has an error of approximately $\pm 0.5m$. Compared with the theoretical floodplain, where the error is in the order of $\pm 1m$, our results show a superior accuracy.

Finally, we apply our methodology to an actual event, the flood damage after the heavy rain in the Omani area, Kyushu region, Japan, in 2019. Fig. 5 shows the comparison of the prediction results and the inundation depth based on human visual inspection using aerial photos published by GSI. In this real-world deployment, our method also yields similar estimates with an error of about 50 cm. These results demonstrated the effectiveness of our methodology and its potential for developing a response system for assessing flood disasters on a nationwide scale.

5. Conclusion

In this article, we developed a methodology that enables rapid estimation of inundation depth following flood disasters. Thus, expanding the current state-of-the-art methods for flood damage assessment, which are mainly limited to estimating flooded areas. Our framework simulated training data using DEM and rainfall scenarios. It trains CNN-based regression models that take a binary mask representing the flooded area and DEM as input and produce inundation depth for a given target area. Experiments based on a real-world disaster response scenario demonstrated the effectiveness of our framework. In our future research, we intend to verify our method using ground truth data collected from other events and increase the number of training areas to scale up the system to function over a much larger area.

Acknowledgments

This work was supported by the Japan Aerospace Exploration Agency (JAXA) 3rd Research Announcement on the Earth Observations, Japan Society for the Promotion of Science through (JSPS) KAKENHI under Grant 22H01741, the Japan Science and Technology Agency (JST), Japan-US Collaborative Research Program, Grant Number JPMJSC2119, and JST, FOREST Grant Number JPMJFR206S.

References

[1] S. Hallegatte, C. Green, R. J. Nicholls, J. Corfee-Morlot, Future flood losses in major coastal cities, Nature Climate Change 3 (2013) 802–806. URL: https://doi.org/10.1038/nclimate1979. doi:10.1038/nclimate1979.

[2] B. Merz, G. Blöschl, S. Vorogushyn, F. Dottori, J. C. Aerts, P. Bates, M. Bertola, M. Kemter, H. Kreibich, U. Lall, E. Macdonald, Causes, impacts and patterns of disastrous river floods, Nature Reviews Earth and Environment 0123456789 (2021). doi:10.1038/s43017-021-00195-3.

[3] L. Moya, E. Mas, S. Koshimura, Learning from the 2018 western japan heavy rains to detect floods during the 2019 hagibis typhoon, Remote Sensing 12 (2020). URL: https://www.mdpi.com/2072-4292/12/14/2244. doi:10.3390/rs12142244.

[4] N. Yokoya, K. Yamanoi, W. He, G. Baier, B. Adriano, H. Miura, S. Oishi, Breaking limits of remote sensing by deep learning from simulated data for flood and debris-flow mapping, IEEE Transactions on Geoscience and Remote Sensing 60 (2022) 1–15. doi:10.1109/TGRS.2020.3035469.

[5] K. Kouchi, F. Yamazaki, Characteristics of tsunami-affected areas in moderate-resolution satellite images, IEEE Transactions on Geoscience and Remote Sensing 45 (2007) 1650–1657. doi:10.1109/TGRS.2006.886968.

[6] S.-W. Chen, M. Sato, Tsunami damage investigation of built-up areas using multitemporal spaceborne full polarimetric sar images, IEEE Transactions on Geoscience and Remote Sensing 51 (2013) 1985–1997. doi:10.1109/TGRS.2012.2210050.

[7] F. Cian, M. Marconcini, P. Ceccato, Normalized Difference Flood Index for rapid flood mapping: Taking advantage of EO big data, Remote Sensing of Environment 209 (2018) 712–730. doi:10.1016/j.rse.2018.03.006.

[8] Y. Li, S. Martinis, M. Wieland, S. Schlaffer, R. Natsuaki, Urban flood mapping using sar intensity and interferometric coherence via bayesian network fusion, Remote Sensing 11 (2019). URL: https://www.mdpi.com/2072-4292/11/19/2231. doi:10.3390/rs11192231.

[9] M. Ohki, T. Tadono, T. Itoh, K. Ishii, T. Yamanokuchi, M. Shimada, Flood Detection in Built-Up Areas Using Interferometric Phase Statistics of PALSAR-2 Data, IEEE Geoscience and Remote Sensing Letters 17 (2020) 1–5. URL: https://ieeexplore.ieee.org/document/8949490/. doi:10.1109/LGRS.2019.2960045.

[10] Y. Bai, W. Wu, Z. Yang, J. Yu, B. Zhao, X. Liu, H. Yang, E. Mas, S. Koshimura, Enhancement of detecting permanent water and temporary water in flood disasters by fusing sentinel-1 and sentinel-2 imagery using deep learning algorithms: Demonstration of sen1floods11 benchmark datasets, Remote Sensing 13 (2021). URL: https://www.mdpi.com/2072-4292/13/11/2220. doi:10.3390/rs13112220.

[11] T. Sayama, G. Ozawa, T. Kawakami, S. Nabesaka, K. Fukami, Rainfall–runoff–inundation analysis of the 2010 pakistan flood in the kabul river basin, Hydrological Sciences Journal 57 (2012) 298–312. doi:10.1080/02626667.2011.644245.

[12] A. Boluwade, Remote sensed-based rainfall estimations over the East and West Africa regions for disaster risk management, ISPRS Journal of Photogrammetry and Remote Sensing 167 (2020) 305–320. URL: https://doi.org/10.1016/j.isprsjprs.2020.07.015. doi:10.1016/j.isprsjprs.2020.07.015.

[13] T. Sayama, Y. Tatebe, Y. Iwami, S. Tanaka, Hydrologic sensitivity of flood runoff and inundation: 2011 thailand floods in the chao phraya river basin, Natural Hazards and Earth System Sciences 15 (2015) 1617–1630. doi:10.5194/nhess-15-1617-2015.

[14] S. Cohen, G. R. Brakenridge, A. Kettner, B. Bates, J. Nelson, R. McDonald, Y.-F. Huang, D. Munasinghe, J. Zhang, Estimating floodwater depths from flood inundation maps and topography, JAWRA Journal of the American Water Resources Association 54 (2018) 847–858. doi:https://doi.org/10.1111/1752-1688.12609.

[15] M. E. Paoletti, J. M. Haut, P. Ghamisi, N. Yokoya, J. Plaza, A. Plaza, U-img2dsm: Unpaired simulation of digital surface models with generative adversarial networks, IEEE Geoscience and Remote Sensing Letters 18 (2021) 1288–1292. doi:10.1109/LGRS.2020.2997295.

[16] O. Ronneberger, P. Fischer, T. Brox, U-net: Convolutional networks for biomedical image segmentation, 2015. doi:10.48550/ARXIV.1505.04597.

[17] B. Adriano, N. Yokoya, J. Xia, H. Miura, W. Liu, M. Matsuoka, S. Koshimura, Learning from multimodal and multitemporal earth observation data for building damage mapping, ISPRS Journal of Photogrammetry and Remote Sensing 175 (2021) 132–143. doi:https://doi.org/10.1016/j.isprsjprs.2021.02.016.

[18] O. Oktay, J. Schlemper, L. L. Folgoc, M. Lee, M. Heinrich, K. Misawa, K. Mori, S. McDonagh, N. Y. Hammerla, B. Kainz, B. Glocker, D. Rueckert, Attention u-net: Learning where to look for the pancreas, 2018. doi:10.48550/ARXIV.1804.03999.

[19] A. Chaurasia, E. Culurciello, LinkNet: Exploiting encoder representations for efficient semantic segmentation, in: 2017 IEEE Visual Communications and Image Processing (VCIP), IEEE, 2017. doi:10.1109/vcip.2017.8305148.

[20] D. P. Kingma, J. Ba, Adam: A method for stochastic optimization, 2014. doi:10.48550/ARXIV.1412.6980.

[21] A. Paszke, S. Gross, F. Massa, A. Lerer, J. Bradbury, G. Chanan, T. Killeen, Z. Lin, N. Gimelshein, L. Antiga, A. Desmaison, A. Köpf, E. Yang, Z. DeVito, M. Raison, A. Tejani, S. Chilamkurthy, B. Steiner, L. Fang, J. Bai, S. Chintala, Pytorch: An imperative style, high-performance deep learning library, 2019. doi:10.48550/ARXIV.1912.01703.

[22] B. Adriano, N. Yokoya, H. Miura, M. Matsuoka, S. Koshimura, A semiautomatic pixel-object method for detecting landslides using multitemporal alos-2 intensity images, Remote Sensing 12 (2020). URL: https://www.mdpi.com/2072-4292/12/3/561. doi:10.3390/rs12030561.

[23] S. Paul, S. Ganju, Flood segmentation on sentinel-1 sar imagery with semi-supervised learning, 2021. doi:10.48550/ARXIV.2107.08369.